

## RESEARCH PAPER

## MODELLING OF LASER POWDER BED FUSION PROCESS FOR DIFFERENT TYPE MATERIALS

Maria Rita Ridolfi<sup>1</sup>, Paolo Folgarait<sup>1</sup>, Andrea Di Schino<sup>2</sup>

<sup>1</sup>Seamthesis Srl, Piacenza, Italy

<sup>2</sup>Università degli Studi di Perugia, Dipartimento di Ingegneria, Perugia, Italy

\*Corresponding author: andrea.dischino@unipg.it, Università degli Studi di Perugia, Dipartimento di Ingegneria, Via G. Duranti 93, 06125 Perugia, Italy

Received: 09.03.2020

Accepted: 10.03.2020

## ABSTRACT

The main problematic coming from the Laser Powder Bed Fusion (L-PBF) technique is the achievement of a fully dense part out of the interconnected tracks. The correct choice of process parameters is of fundamental importance to obtain a porosity free component. In this work, a model is described as able to simulate the printing process. The proposed model is a simplified numerical tool for designing processing windows suitable for metal alloys of any composition. The considered approach makes the model used as much practical as possible while keeping the physical description representative. The model is validated fitting experimental measures of track width, depth and cross-sectional area taken from three literature sources, referring to Ti6Al4V, Inconel 625 and Al7050. Effective liquid pool thermal conductivity, laser absorptivity and depth of application of laser energy are here considered as fitting parameters. Laser absorptivity and depth of application of laser energy result to rise almost linearly with increasing specific energy; the slopes of the three analyzed alloys result very close to each other. The obtained results give confidence about the possibility of using the model as a predicting tool after further calibration on a wider range of metal alloys.

**Keywords:** selective laser melting; additive manufacturing; modelling

## INTRODUCTION

Laser Powder Bed Fusion (L-PBF) is one of the most adopted and successful powder bed fusion-based additive manufacturing technologies for many types of alloys including stainless steels and light alloys [1-6]. In L-PBF melting and solidification of a small powder, the volume is obtained using scanning on a powder layer by a laser. In the end, the partially overlapping tracks solidified or partially re-melted on any single layer are connected and the final component is manufactured. Main critical issues coming from this method concern the achievement of a fully dense part out of tracks interconnections. The target mechanical properties of a component (*e.g.* strength, ductility, creep and fatigue behaviours) strongly depend on the presence of porosities [7-18]. It is well known that process parameter correct determination a key issue to achieve porosity-free manufacture. It is also known that it strongly depends on powder composition morphology. The process parameter list includes the following topics: layer thickness, hatch, laser spot diameter and power. Finally, scanning speed needs to be considered. While layer thickness is affected by matters depending on the component target surface finishing degree resolution, the laser spot diameter is usually fixed on commercial 3d printers. The optimized process needs to take into account the determination of the best laser power and speed as well of the hatch distance. Therefore in order of selective laser melting process optimization, tools able to define the operating window in the  $P$ - $v$  (laser beam power – velocity) space are needed. Such tools are required to take into account the dependence of such items on metals composition and powder morphology.

Several approaches have been developed for the above problem [19-22]. In the approach reported in [23], the process mapping simply gets to the process outcomes of an additive manufactured process, just considering input power and speed. Usually, constant cross-sectional area curves are plotted to allow to determine the power and speed combinations resulting in a similar melt pool cross-sectional area.

Numerical modelling of the track melting has been approached by the use of commercial finite element software's [24-26].

In particular [27] reports about experiments carried out at the National Institute of Standards and Technology (NIST) on an Inconel 625 plate using an EOSINT M270 Laser Powder Bed machine. A test matrix of several powers and speed values combinations was originated, covering the full standard operating region of the considered 3D printer. Laser process simulations were carried out using a 3D finite element model. Results of the simulation were compared with the experimental cross-sectional areas. A not perfect fitting was obtained using a fixed value of effective laser absorptivity of 0.57, inducing to hypothesize better fitting for an absorptivity varying with laser power and speed.

In this paper, we propose a modelling tool able to generate processing maps of alloys suitable to the laser powder bed fusion technique. A simplified physical frame is modelled to reduce computing time. The model is then applied covering process parameters ranges typical of the specific additive manufacturing machine. The output is the limits of the conduction, transition and keyhole modes in the laser power-velocity plane, along with the full dense region.

Experimental data concerning different thermo-physical alloys properties are needed to validate the model. Three data sources have been selected throughout the literature at this first step of the model evolution [28-33].

## The model

The continuous modification of the melt pool as the specific laser energy is due to the gas/melt surface evaporation onset and occurs when the temperature is high enough. The conduction mode ends up and a recoil momentum [10] is produced modifying the initially flat gas/melt interface and leading to an increasingly deeper cavity as the laser entering specific energy is enhanced. As the cavity deepens, higher energy values are absorbed into the cavity due to multiple ray reflections against the cavity interface [29]. Due to this mechanism, a shallow

cavity intercepts less energy than a deep keyhole cavity, resulting in a continuous increase of the effective laser absorbance of the interface achieving its minimum in the conduction mode; afterwards increasing in the transition mode, until reaching the maximum close to unity, for a fully developed keyhole. The absorbance minimum value is strictly correlated to the natural absorptivity of the metal alloy. As a consequence, the melt pool geometry transforms turning from wide and flat into narrow and deep.

The model is developed using the finite volume technique aimed to better take into account the gas cooling effect and its dependence on its vector properties and is described in detail in [34].

To achieve a simplified representation of the welding process, two main assumptions are performed:

1. avoiding evaporation and keyhole formation of explicit simulation. Heat transfer is modelled in terms of conduction through the melt pool for any operating condition input. This implies an accurate model validation and calibration for properly taking into account how much evaporation and formation of the cavity affect the melt pool geometry and overall heat transfer conditions.
2. modelling the powder layer as a continuum material, which thermo-physical properties come from a local powder particles arrangements, leading to the formation of sites where the powder is packed or rarefied (as the effect of the mixture with the gas).

**RESULTS**

The first applications, herein discussed, refer to single tracks generated over a single powder layer and have been used to calibrate the model using consistent experimental data [27-29].

The applied strategy to gain fitting results involves two different stages. In the first stage, the input laser specific energy is raised from the lowest level, the height  $h$  is set to an initial value and the laser absorptivity is given as first attempt the value competing to the simulated metal alloy, as deduced from available databases of metal surfaces reflectivity. Both  $h$  and  $\alpha$  keep constant values for all operating conditions resulting in conduction mode.

The calibration when simulating the conduction mode is addressed at fitting measured depth and width data and at obtaining the boiling conditions in the weld pool at operating conditions experimentally marking the passage from conduction to evaporation. Experimental data employed in this work provide numerous track measures at different  $P$ - $v$  values, scanning over the operating ranges of  $P$  and  $v$  with quite fine resolution, allowing for precisely detecting the transition from conduction to evaporation and keyhole formation. Laser absorptivity and effective thermal conductivity in the liquid pool are set as fitting parameters. Up to now, the calibration experience shows almost no need to vary the laser absorptivity derived from literature and web repositories referring to each metal alloy.

In the second stage, height  $h$  and  $\alpha$  are varied with varying laser parameters until fitting measured values of depth and width. In particular, absorptivity increases with increasing the input laser specific energy until reaching a plateau at a value close to unity. Laser efficiency  $\eta$  has been kept constant and equal to 0.85.

The comparison between measured and calculated cross-sectional data are reported in Figure 1, in terms of width and depth data concerning the analysis performed on Ti6Al4V [28] (Figure 1a), Inconel 625 [29] (Figure 1b) and of the cross-sectional area for Al7050 [27] (Figure 1c).

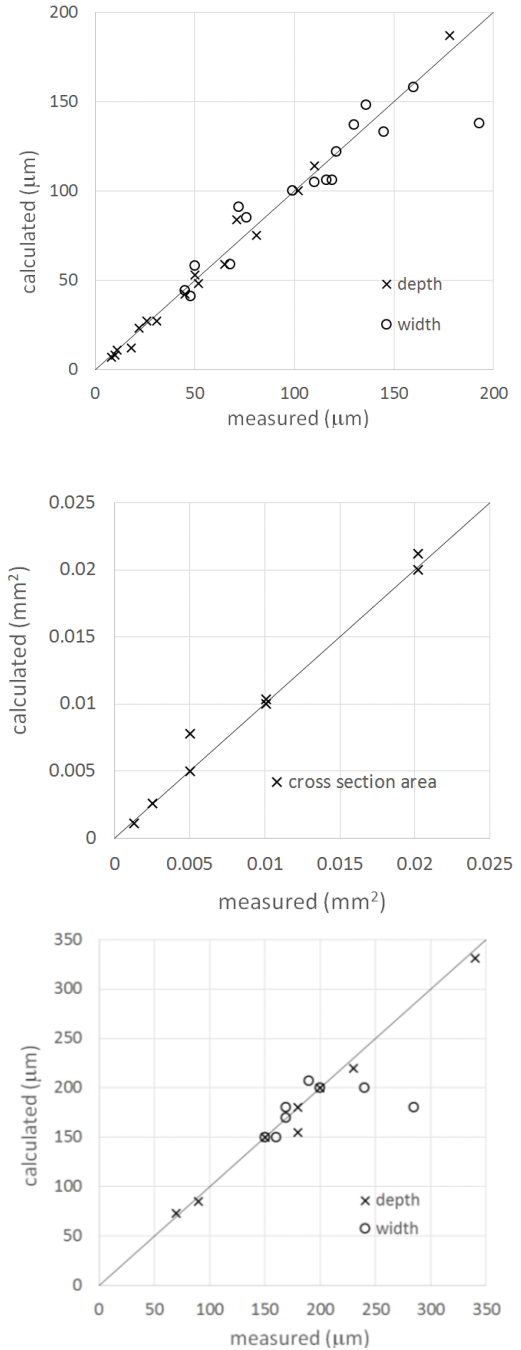


**Fig. 1** Comparison between measured and calculated data of Ti6Al4V track depth and width (a), Inconel 625 track cross-section area from (b), Al7050 (c).

A good agreement has been found except for width values for deep keyhole shapes. The typical keyhole cross-section geometry is characterised by a width profile rapidly changing from wide, near the surface, to narrow deep below. The simplified approach of the present model is not capable to catch this geometry complexity. The net result is that it fails in giving precise width values, although the calculated depth and cross-sectional area fit well the measured values.

The fitting parameters:  $h$  and  $\alpha$  shows the trends against specific energy,

shown respectively in Figure 2 and Figure 3.

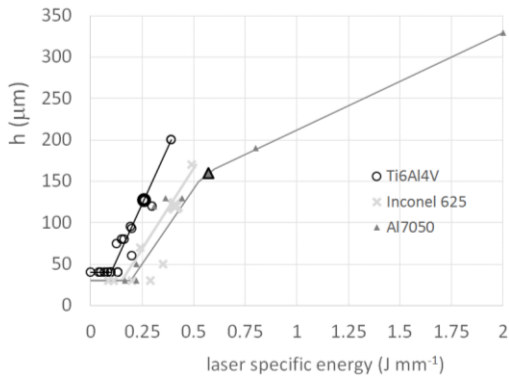


**Fig. 2.** Calculated trends of height  $h$  vs specific energy for the three analysed alloys.

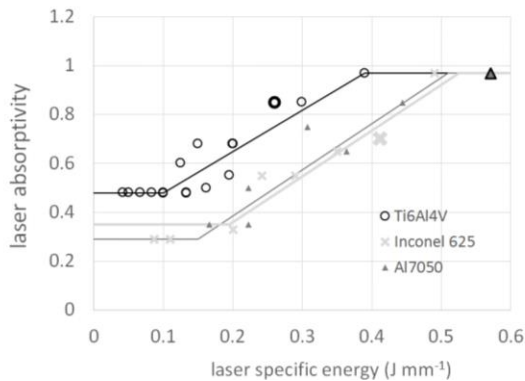


**Fig. 2.** Calculated trends of laser absorptivity vs specific energy for the three analysed alloys.

Bold symbols in Figure 2 and 3 highlight specific energies above which deep keyhole is experimentally observed for the three alloys. Dilip et al. [28] put into evidence the presence of keyhole porosity for specific energies above  $0.26 \text{ J mm}^{-1}$ . Montgomery et al. [27] notice keyhole shape for specific energies above  $0.4 \text{ J mm}^{-1}$  and Qi et al. [29] recognise well-developed keyhole regime only at very high power level, close to  $2 \text{ J mm}^{-1}$ , although severe keyholing is detected at specific energy as low as  $0.57 \text{ J mm}^{-1}$ .

While for Ti6Al4V and Inconel 625 this experimental outcome meets the respective calculated curves at  $\alpha \approx 0.8$ , the keyhole observed in Al7050 tracks appears for a calculated  $\alpha = 0.97$ .

## CONCLUSION

A model has been developed using the commercial code ANSYS Fluent for simulating the printing process inside an L-PBF machine. A simplified approach has been adopted to make the model use as much practical as possible for design the processing window of alloys of any composition.

The model has been calibrated fitting experimental measures of track width, depth and cross-sectional area taken from three literature sources, referring to Ti6Al4V, Inconel 625 and Al7050.

A strategy of model calibration is employed based on varying the effective liquid pool thermal conductivity to fit the experimentally observed evaporation start with the calculation of the boiling temperature as maximum pool temperature. Laser absorptivity and depth of application of laser energy are further varied to fit width and depth data. They result to rise almost linearly with increasing specific energy assuming slopes very close for the three analyzed alloys. In particular, laser absorptivity increase from the base level consistent with the absorptivity of the alloy at the laser wavelength, until reaching a maximum value close to unity. From the experiments described in the reference papers used in this work, deep keyhole already appears for calculated values of absorptivity of almost 0.8. The model needs to be further calibrated to validate the present observations and refine the fitting parameters (effective liquid conductivity, the slope of  $h$  and  $\alpha$ ).

## REFERENCES

- P. Petrousek et al.: Acta Metallurgica Slovaca, 25, 2019, 283-290. DOI: 10.12776/ams.v25i4.1366
- L. Parilak, E. Dudrova, R. Bidulsky, M. Kabatova: Powder Technology, 322, 2017, 447. DOI: 10.1016/j.powtec.2017.09.027
- D. Manfredi, R. Bidulsky: Acta Metallurgica Slovaca, 23(3), 2017, 276-282. DOI: 10.12776/ams.v23i3.988.
- A. Di Schino, L. Valentini, J.M. Kenny, Y. Gerbig, I. Ahmed, H. Haefke: Surf. Coat. Technol., 161, 2002, 224-231. DOI: 10.1016/S0257-8972(02)00557-1.
- G. Bregliozzi, A. Di Schino, J.M. Kenny, H. Haefke: Materials Letters, 57, 2003, 4505-4508. DOI: 10.1016/S0167-577X(03)00351-3
- G. Napoli, M. Paura, T. Vela, A. Di Schino, Metalurgija, 57, 2011, 111-113.
- R. Bidulsky et al.: Acta Physica Polonica A, 128(4), 2015, 647-650. DOI: 10.12693/APhysPolA.128.647
- H.W. Mindt, O. Desmaison, M. Megahed, A. Peralta, J. Neumann: Journal of Materials Engineering and Performance, 27, 2018, 23-43. DOI: 10.1007/s11665-017-2874-5
- H. Gong, K. Rafi, H. Gu, T. Stucker: Additive Manufacturing, 2014, 1-4, 87-98. DOI: 10.1038/s41598-019-54293-w
- S. Khairallah, A. Anderson, T. Wayne, R. King: Acta Materialia, 108, 2016, 36-45. DOI: 10.1016/j.actamat.2016.05.017
- C. Zitelli, P. Folgarait, A. Di Schino: Metals, vol. 9, 2019, 731. DOI: 10.3390/met9070731.
- A. Di Schino, P.E. Di Nunzio: Acta Metallurgica Slovaca, 23, 2017, 62-71. DOI: 10.12776/ams.v23i1.852.
- R. Bidulsky, M. Actis Grande, E. Dudrova, M. Kabatova, J. Bidulska: Powder Metallurgy, 59(2), 2016, 121-127. DOI: 10.1179/1743290115Y.0000000022.
- A. Di Schino, M. Longobardo, G. Porcu, G. Turconi, L. Scoppio: NACE – International Conference Series 2006, 062151-06125114.
- A. Di Schino: Acta Metallurgica Slovaca, 22, 2016, 266-270. DOI: 10.12776/ams.v22i4.815
- A. Di Schino, P. Di Nunzio, G.L. Turconi, Materials Science Forum, 558-559, 2007, 1435-1441. DOI: 10.4028/0-87849-443-x.1435.
- G. Bregliozzi, S.I.U. Ahmed, A. Di Schino, K.M. Kenny, H. Haefke: Tribol. Lett., vol. 17, 2004, 697-704.
- J. Bidulska, T. Kvackaj, I. Pokorny, R. Bidulsky, M. A. Grande: Archives of Metallurgy and Materials, 58, 2013, 371-375. DOI: 10.2478/amm-2013-0002
- J. Bidulska, R. Bidulsky, T. Kvackaj, M. A. Grande: Materials, 12, 2019, 3724. DOI: 10.3390/ma12223724.
- D. Almangour, D. Grzesiak, J. Cheng, Y. Ertas: Journal of Materials Processing Technologies, 257, 2018, 288-301- DOI: 10.1016/j.jmatprotec.2018.01.028

21. T. Bartel, I. Guscke, A. Menzel: Computer and Mathematic with applications, 78, 2019, 2267-2281  
DOI:10.1016/j.camwa.2018.08.032
22. M. Schanzel, D Shakirow, A. Ilin, V. Ploshikhin: Computer and Mathematic with applications, 78, 2019, 2230-22461  
DOI:10.1016/j.camwa.2018.01.019.
23. J. Beuth, N. Klingbeil: JOM, 53, 2001, 36-39.
24. R. Ruffini, O. Di Pietro, A. Di Schino: Metals, 8, 2018, 519.  
DOI: 10.3390/met8070519.
25. A. Di Schino, J.M. Kenny, G. Abbruzzese: J. Mater. Sci., 37, 2002, 5291-5298.  
DOI: 10.1023/A:1021068806598.
26. A. Di Schino, J.M. Kenny, I. Salvatori, G. Abbruzzese: J. Mater. Sci., 36, 2001, 593-601.  
DOI: 10.1023/A:1004856001632.
27. C. Montgomery, J. Beuth, L. Sheridan, N. Klingbeil: Proceedings of the Annual International Solid Freeform Fabrication Symposium, 2015, 1195–1204.
28. J. Dilip, S. Zhang, C. Teng, K. Zeng, C. Robinson, D. Pal, B. Stucker: Progress in Additive Manufacturing, 2, 2017, 157–167.  
DOI: 10.1007/s40964-017-0030-2
29. T. Qi, H. Zhu, H. Zhang, J. Yin, L. Ke, X. Zeng: Materials & Design, 2017.  
DOI: 10.1016/j.matdes.2017.09.014.
30. W. King, H. Barth, V. Castillo, G. Gallegos, J. Gibbs, D. Hahn, C. Kamath, A. Rubenchik: Journal of Materials Processing Technology, 214, 2014, 2915–2925.
31. M. Maina, R. Okamoto, R. Inoue, S. Nakashiba, A. Okada, T. Sakagawa.: Appl. Sci., 8, 2018, 1-13.  
DOI: 10.3390/app8122364
32. T. Mukherjee, J. Zuback, S. De, T. DebRoy, 7th International Symposium on High-Temperature Metallurgical Processing, 2016, 471-478.
33. L. Viet, J. Hye-Jin: Metals, 8, 2018, 815.  
DOI: 10.3390/met8100815
34. M. Ridolfi, P. Folgarait, V. Battaglia, T. Vela, D. Corapi, A. Di Schino: Procedia Structural Integrity, 24, 2019, 370-380.  
DOI: 10.1016/j.prostr.2020.02.034